



Experimental Investigations of 3D-Deformations in Additively Manufactured Pantographic Structures

Gregor Ganzosch¹(✉), Emilio Barchiesi², Rafal Drobnicki³, Aron Pfaff⁴,
and Wolfgang H. Müller¹

¹ Department of Mechanics, Chair of Continuum Mechanics and Constitutive Theory, Berlin University of Technology, Einsteinufer 5, 10587 Berlin, Germany
ganzosch@tu-berlin.de

² Dipartimento di Ingegneria e Scienze dell'Informazione e Matematica, Università degli Studi dell'Aquila, Via Vetoio 1, Coppito, 67100 L'Aquila, Italy

³ Institute of Mechanics and Printing, Warsaw University of Technology, 85 Narbutta Street, 02-524 Warsaw, Poland

⁴ Additive Design and Manufacturing, Fraunhofer Ernst Mach Institute, Ernst-Zermelo-Straße 4, 79104 Freiburg, Germany

Abstract. In the recent past new experimental techniques have been developed with the objective of linking generalized continuum theories with technology. So-called pantographic structures, which can be characterized as a meta-material, will be presented and investigated experimentally: Samples of different materials and dimensions are subjected to large deformation loading tests (tensile, shearing, and torsion) up to rupture, while their response to loading is recorded by an optical measurement system. 3D-digital image correlation is used to quantify the deformation.

Results show that the deformation behavior is strongly non-linear and that the structures are capable of performing large (elastic) deformations without complete failure. This extraordinary behavior makes pantographic structures very attractive as engineering material in technical applications for lightweight applications and in the medical industry.

Keywords: Experiment · Metamaterial · Digital image correlation · Additive manufacturing

1 Introduction

With the help of additive manufacturing fabrication of complex designed structures became cheaper over the last decades. Developments and implementations of customized substructures in combination with specially tailored materials became possible resulting in extraordinary macroscopic deformation behavior. Such a man-made structure is also referred to as a meta-material. Pantographic structures, which can be described as meta-materials with a substructure composed of two orthogonal arrays of beams, connected by internal cylinders or

joints (see Fig. 1), were manufactured by using additive manufacturing techniques. Such meta-materials enable the fabrication of lightweight structures with high degrees of complexity in combination with high stiffnesses. Effective properties are carefully designed by tailoring the so-called microscopic constituents [3, 17, 18] in the substructure in order to achieve specially desired properties, where the unit cells of the substructures are repeated periodically. Therefore mechanical performance of meta-materials depends not only on the global structure, but also on the morphology of their subunits.

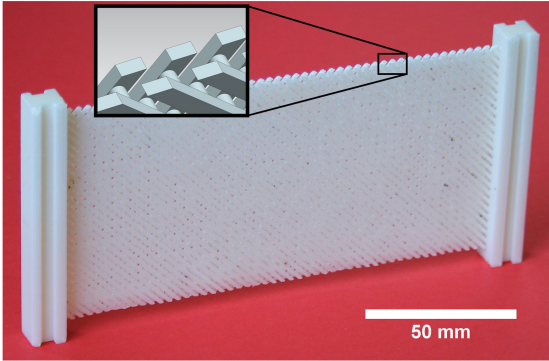


Fig. 1. Pantographic structure developed by [8] made out of polylactide, manufactured at the Institute of Mechanics at Technische Universität Berlin by means of fused deposition modeling technique.

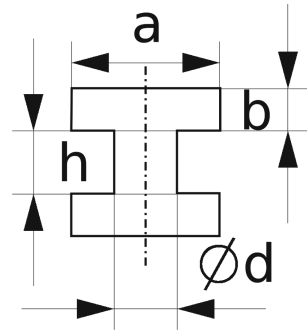


Fig. 2. Two-dimensional cross-section of an unit cell of a pantographic substructure.

The design and manufacture of meta-materials for specific engineering applications requires us to predict their performance. This can be achieved by the finite element method [5, 35, 39]. Normally the modeling of technical structures is based on the equations of the traditional CAUCHY-BOLTZMANN continuum. This requires a very detailed mesh if details need to be analyzed, which leads to higher computing time and associated higher costs. Alternatively, by using equations developed from generalized continuum theories, a low-detail mesh can be used to get the same results and, correspondingly, the computational costs are much less. The classical first gradient Cauchy theories need to be improved by introducing either additional degrees of freedom, for example those of the COSSERAT medium [6, 7], micropolar parameters [13, 14, 29, 30], or additional higher order gradients [1, 2, 9, 24, 25, 27, 31, 32, 36].

It is known that pantographic structures can be represented well by higher gradient theory. In fact they were treated as a second gradient continuum [3, 10]. Here, the bending stiffness of the fibers is described by a second-gradient dependence (in displacement). However, new material parameters are introduced into the constitutive laws and experiments have to be designed to calibrate and determine these parameters [4, 16]. By choosing a specially adjusted experimental setup in combination with an explicit theory it is possible to localize and

to determine the unknown parameters [8, 20–24, 38]. On the one hand side one may say that newly identified parameters gained from theory have to be measured and determined in experiments [23, 24, 26], and on the other hand side the parameters obtained from theory or numerical analysis have to be validated by experiments [8, 25, 37].

In this paper three types of experiments applied to meta-materials made out of three different materials consisting of pantographic substructure will be performed. In addition a non-invasive optical measurement technique, the so-called Digital Image Correlation (DIC), will be used to detect and to measure the deformation on the specimens' surface. Pantographic metamaterials show a highly resilient and non-linear elastic material behavior resulting in large deformations.

2 Materials and Methods

Different materials and different experimental setups have been taken into account in this work. Three different additive manufacturing procedures were used to manufacture three differently sized samples, which will be described in Subsect. 2.1. Standardized test-setups of three different experimental methods will be presented in detail in Subsect. 2.2.

2.1 Manufacturing

Pantographic structures, consisting of rectangular beams and cylindrical pivots/joints, were 3D-printed using three different additive manufacturing methods:

- i) Fused Deposition Modeling (FDM) by means of an Ultimaker 3 Extended (Ultimaker B.V., Geldermalsen, Netherlands) available at Technische Universität Berlin, Chair of Continuum Mechanics and Constitutive Theory, Germany,
- ii) Selective Laser Sintering (SLS) by means of EOS Formagia P 100 (EOS GmbH, Munich, Germany) located at University of Technology Warsaw, Institute of Mechanics and Printing, Poland,
- iii) Direct Metal Laser Sintering (DMLS) by means of EOS M 400 (EOS GmbH, Munich, Germany) located at Fraunhofer Ernst-Mach-Institute Freiburg, Germany.

Polylactic Acid (PLA - Ultimaker B.V., Geldermalsen, Netherlands) was used as raw material for FDM (specimen **PLA**). In order to increase the printing quality of the specimen, water-soluble Polyvinyl Acetate (PVA - Ultimaker B.V., Geldermalsen, Netherlands) was used additionally as support-structure during the



Fig. 3. Speckled pantographic structures made out of PLA (left), PA (middle), and AlSi10Mg (right).

printing process and was washed off afterwards (for further informations see [19]). Polyamide (PA2200 - EOS GmbH, Munich, Germany) was used as raw material in SLS (specimen **PA**). For further informations see [4, 15]. Aluminium alloy (AlSi10Mg - EOS GmbH, Munich, Germany) was used as raw material using DMLS (specimens **ALU**, **ALU-H**). A special support structure and a complicated elaborated laser exposure strategy was employed in order to avoid thermal distortions due to the higher laser powers and energy input. Furthermore, a heat treatment was performed on sample **ALU-H** in order to reduce internal stresses (for further informations see [16]). Since the microscopic substructures influence the macroscopic deformation behaviors significantly [4, 33], variations of specimens with different geometries were investigated as well. Figure 3 shows three types of specimens (sample **PLA**, **PA**, and **ALU**). In total four different specimens were investigated:

- 1) sample **PLA** in extension,
- 2) sample **PA** under shear,
- 3) sample **ALU** torsion-test,
- 4) sample **ALU-H** torsion-test.

Details of the inner and outer dimensions of all samples can be found in Table 1.

Table 1. Outer dimensions in mm (L = width, l = height, t = depth) of all samples as well as inner dimensions of the substructure of all samples corresponding to the schematic in Fig. 2 (a = width of beam, b = height of beam, $\varnothing d$ = diameter of pivot, h = height of pivot).

Sample	L	l	t	a	b	$\varnothing d$	h
PLA (extension)	140	70	3	1	1	1	1
PA (shear)	210	70	3	1	1	0.9	1
ALU (torsion)	210	70	5	1	1	0.9	3
ALU-H (torsion)	210	70	5	1	1	0.9	3

2.2 Experimental Setup

The experiments can be classified as extension, torsion and shearing tests. Extension tests have been performed on a MTS Tytron 250 testing device at Technische Universität Berlin, Chair of Continuum Mechanics and Constitutive Theory (CMCT). Torsion- and shearing-tests have been performed on a Zwick Z010 at Charité Berlin, Julius Wolff Institute (JWI) respectively. Quasi-static standard tests have been taken into account. The experimental setup of extension tests performed on sample **PLA** at CMCT is shown in Fig. 6A; the experimental setup of shearing-test performed at JWI is presented in Fig. 4. In this work we will also focus on torsion tests applied to **ALU** and **ALU-H** specimens. The schematic setup of torsion-test performed at JWI is shown in Fig. 5.

The MTS Tytron 250 testing-device controlled by the software Stationsmanager V 3.14 was used during extension tests on sample **PLA**. The applied force was measured by a load cell attached to the device, which is able to record axial forces in a range of $F = \pm 250$ N. The displacement, x , was imposed horizontally on the right of the specimen with a loading rate of $v = 15$ mm/min (displacement-controlled). It was measured and monitored by the device's own encoder unit. Almost frictionless movement was achieved by using an air-film-bearing. External vibration was avoided by using a massive substructure and by arranging the system horizontally. Additionally to force-displacement (stress-strain) recording, pictures were taken (0.25 pictures/second) by means of a commercial Canon EOS 1000D camera with a resolution of 4272×2848 pixels. Triggered pictures and force/displacement were synchronized with the help of a TTL signal. 2D-DIC evaluation was performed in GOM Correlate 2017 software (GOM GmbH, Braunschweig, Germany).

For investigating specimens made out of aluminum (samples **ALU** and **ALU-H**), which need higher loads to generate measurable results, the Zwick Z010 testing-device, controlled by the software TestExpert was used. The shearing-tests on the **PA** sample were also performed with this device. The resultant

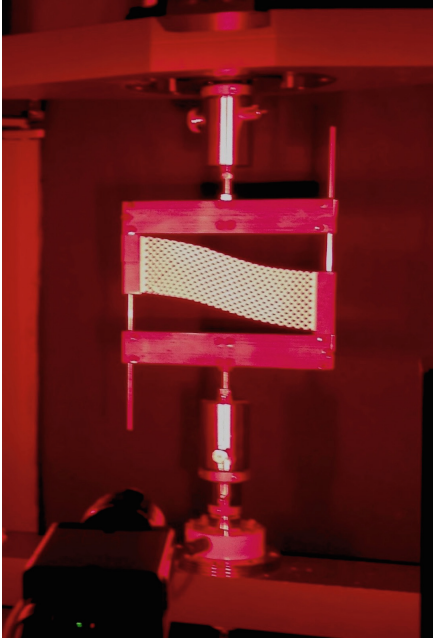


Fig. 4. Set-up of shear experiment of sample PA performed on the Zwick Z010 device at JWI (for further informations of experimental setup see [16]).

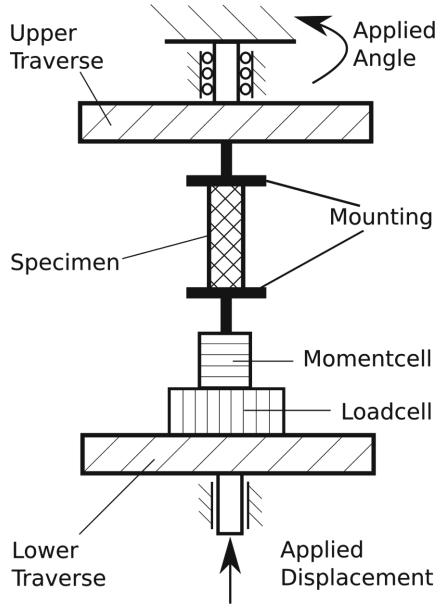


Fig. 5. Schematic set-up of extension and torsion experiments performed on the Zwick Z010 device.

applied axial force was measured by a device-own load cell (Zwick-Serie Xforce). The force transducer is able to record axial forces in the range of about $F = \pm 10000$ N, where the accuracy at 20 N is about 0.1%. The displacement x was controlled vertically. The upper traverse-part of the tensile-to-shear adaption device is fixed horizontally and vertically, while the lower part can be linearly moved in the vertical direction (see Fig. 5). The velocity of the shearing-test was set to $v = 15$ mm/min, which is quite slow for such tests (displacement-controlled and quasi-static). The displacement itself was recorded and monitored by a device-own encoder unit with an accuracy of ± 0.002 mm. For the torsion tests a device-own torque sensor (Zwick-Serie M) was applied on the very fixed bottom of the lower traverse, while the torsion was induced on the top of the mounting with 1 degree/min on the upper traverse-part of the torque adaption-device (see Fig. 5). The torsion transducer is able to record moments up to $M = 20$ Nm and resists maximal axial forces up to ± 5 kN. Furthermore a non-invasive optical measurement device Q-400 (Dantec Dynamics GmbH, Ulm, Germany) was installed to record the state of three dimensional deformation of the surface of a sheet by the help of two cameras. A more-than-one camera system is able to recognize the 3D-motion within overlapping regions of the image sections. For

enable the software of image correlation to separate small surface areas (so-called facets) and due to lack of contrast, the surfaces of all specimens had to be sprayed with a speckled pattern (see Fig. 3). During the deformation process, pictures were taken via direct TTL-signal every 2 s by means of the afore mentioned commercial camera system with a resolution of about 1600×1200 pixels. This way we were able to synchronize each picture to the related force-value in real time. By means of a calibration procedure of the camera setup, the commercial software Istra4D is able to re-calculate a three dimensional surface deformation.

3 Results

In order to obtain scalar results for an out-of-plane displacement of a sheet in DIC, a reference point in a single facet (a sub-area of image correlation) was selected for each sample. This point is located in the place where maximal out of-plane movement could be assumed. Due to the large deformations some facets moved out of the optical focus, which caused the image correlation to abort. Furthermore, image correlation may also be aborted when a sudden rupture occurs in between the shutter releases of the camera, so that the facets to be correlated are displaced too much. For further informations see [16, 19]. Torsion tests applied to the aluminum specimens were performed on the same experimental setup with identical loading conditions.

3.1 Extension

The extension test with the **PLA** sample was performed on a MTS Tytron 250 device located at Institute of Mechanics at Technische Universität Berlin, Germany. Figure 7 shows the stress-strain relation of sample **PLA** in a biaxial tension test. The marked points **A**, **B**, and **C** correspond to the sequence pictures in Fig. 6, respectively. After linear elastic deformation (between points **A** - **B**), plastic deformation occurs resulting in a first rupture shortly after an elongation of about $\varepsilon = 6\%$, which is a quite low elongation for pantographics (see [16, 34]). The pivot in the lower right corner breaks (Fig. 7C), but surprisingly total failure can be avoided. The structure is even able to resist higher loads after a second rupture. Necking, calculated by means of 2D-DIC in vertical direction, results in a shortening in vertical direction of about $\Delta y = 5$ mm and is shown in the right lower corner in Fig. 6. Obviously, high elastic performance as seen in previously investigated experimental studies [4, 8, 11, 15, 16, 34] has not been experienced with this specimen because of the small height of the cylindric pivot/joint (see [34]).

3.2 Shearing

Shearing tests with the **PA** sample were performed on a Zwick Z010 testing device at the Julius Wolff Institute at Charité Berlin, Germany (see Fig. 4).

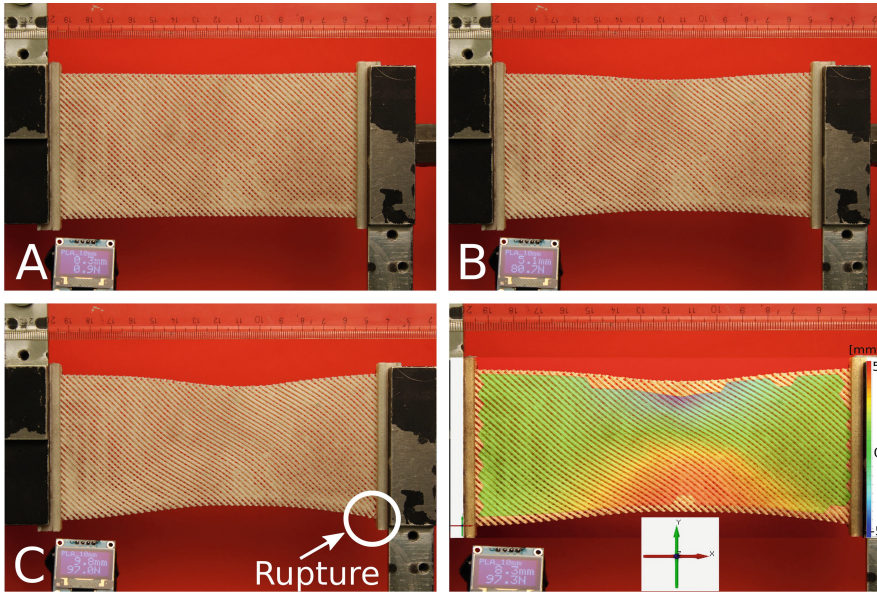


Fig. 6. Image sequence of specimen **PLA** during extension load. Picture **A - C** correspond to the marked points in Fig. 7. The picture in the lower right corner shows exemplarily the calculated necking in *y*-direction by means of 2D-DIC shortly before first rupture occurs.

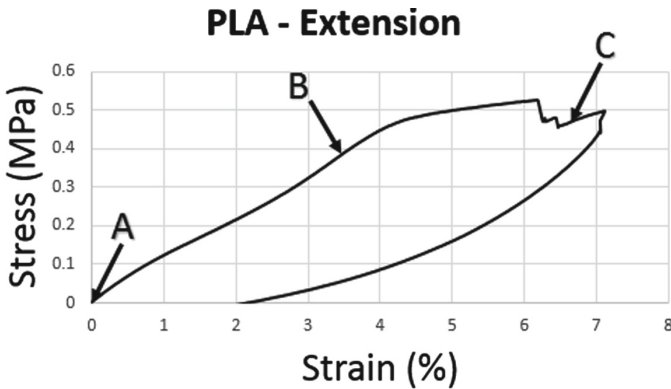


Fig. 7. Stress-strain curve of biaxial extension test of specimen **PLA** performed on MTS Tytron 250 device at CMCT. Arrows pointing to points **A**, **B**, and **C** correspond to pictures **A**, **B**, and **C** in Fig. 6, respectively.

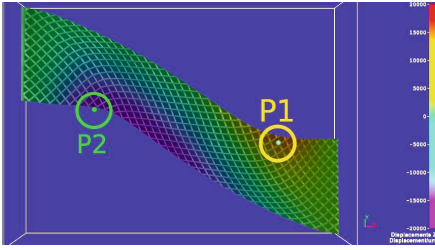


Fig. 8. 3D-DIC evaluation of specimen **PA** during shearing test with positive (red, point P1) and negative (blue, point P2) out-of-plane-movements.

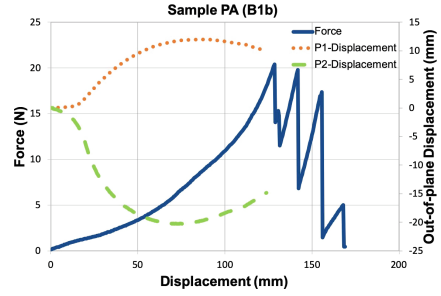


Fig. 9. Shear-force-displacement relation of specimen **PA** including asymmetric out-of-plane-movements of points P1 (positive) and P2 (negative), respectively.

Figure 8 shows the out-of-plane movement of the surface of sample **PA** during the shearing test. Because of the stiffness of pivots/cylinders (see [4, 34]), which connect the arrays of beams of the different planes, out-of-plane buckling occurs, being in good agreement with previous investigations reported in [4, 15, 16]. In Fig. 9 out-of-plane movements of the points P1 and P2 corresponding to Fig. 8 and the force-displacement curve are shown. An almost linear elastic deformation behavior can be observed until about $y = 50$ mm (shear elongation of $\Delta e_{yy} = 71\%$). Surprisingly, strongly non-linear and non-symmetric out-of-plane movements start at about $y = 10$ mm while being still in the linear elastic deformation range ($\Delta y < 50$ mm). After reaching a maximal shear-displacement at about $y_{max} = 70$ mm the out-of-plane buckling decreases. This is because of the high plastic deformation in the structure. One may say that the “shearing test becomes an elongation test” at this very point.

Furthermore, the first rupture occurs at about $y = 127$ mm of shear-deformation (shear elongation of $\Delta e_{yy} = 181\%$) at almost 21 N. The whole metamaterial is able to resist even further loading without leading to total failure resulting in a high resilient-kind deformation behavior. Even after the fourth rupture at about $y = 155$ mm shear-displacement (shear elongation of $\Delta e_{yy} = 221\%$), the whole structure does not fail and is able to resist higher loads up to 5 N before total failure.

3.3 Torsion

Torsion tests applied to sample **ALU** and sample **ALU-H** were performed on a Zwick Z010 testing device at Julius Wolff Institute at Charité Berlin, Germany. Figure 10 shows the heat-treated specimen sample **ALU-H** after one total rotation (360°). Figure 11 shows the out-of-plane buckling of the same specimen right after first torque was applied at the upper mounting part. The points P1 and P2 show about ± 14 mm out-of-plane movement before the facets got lost

and DIC-evaluation was aborted. In Fig. 12 moment-, angle-, and out-of-plane movement-time relations are shown. Linear elastic as well as linear plastic deformation behavior was observed. In order to investigate the plastic deformation of both specimens, rotations with load cycles of 10° steps were imposed up to 60° ($0^\circ - 10^\circ - 0^\circ - 20^\circ - 0^\circ - \dots - 60^\circ - 0^\circ - 2000^\circ$). By reaching the negative area ($F < 0\text{ Nm}$) after the 20° step plastic deformation clearly occurs. Furthermore, non-linear deformation behavior can be recognized after 60° (at about 480 s).



Fig. 10. Sample **ALU-H** after one full rotation during torsion test performed on Zwick Z010 at JWI, Charité in Berlin, Germany.

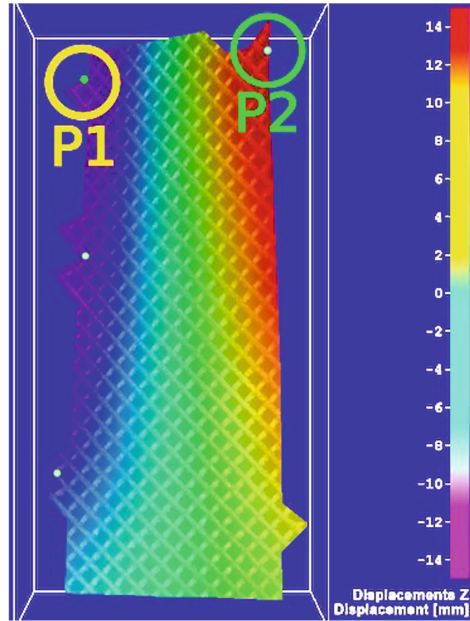


Fig. 11. Example of 3D-DIC evaluation of specimen **ALU-H** during torsion test with negative out-of-plane-movement (blue, point P1) and positive out-of-plane-movement (red, point P2).

By comparing the moment-time dependencies of the heat-treated specimen, **ALU-H**, with the untreated one, **ALU**, in Fig. 13, considerable differences in the deformation behavior can be observed. The specimen **ALU** reaches about 16% higher loads than the heat-treated one, **ALU-H**. But sample **ALU-H** is able to resist further loads without leading to a single failure because of its ductility. This is in contrast to sample **ALU**, in which local ruptures of beams and pivots result in total failure. But still, **ALU** was able to resist even higher torque-loads before total failure of the whole structure occurred. This resilient deformation behavior was also observed in the aforementioned extension test applied to specimen **PLA** and in the shearing test applied to specimen **PA**.

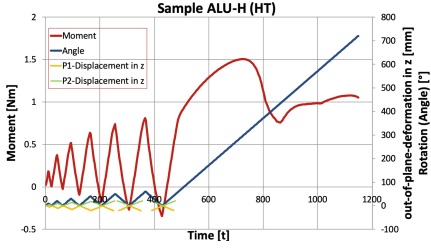


Fig. 12. Diagram of moment-, angle-, and out-of-plane movement over time of torqued specimen **ALU-H**.

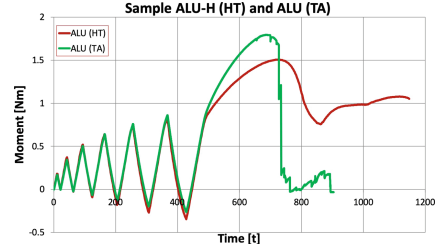


Fig. 13. Comparison of moment-time dependences of specimens **ALU-H** and **ALU** during a torsion test.

A reverse POYNTING effect was observed and is further discussed in [28] and [12]. It should also be mentioned that total failure of the heat-treated specimen **ALU-H** did not occur during the whole experiment ending after 5.7 total rotations (about 2000°). This extraordinary deformation behavior is comparable to investigations with cylindrical structures reported in [12].

4 Conclusion and Outlook

Pantographic structures made out of three different materials were additively manufactured using three differently types of additive manufacturing techniques. Polylactide was used as a raw material for 3D-printing of specimen **PLA** by means of fused deposition modeling at Technical University Berlin, Germany. Polyamide was used as a raw material for 3D-printing of specimen **PA** by means of selective laser sintering at Polytechnica Warsaw, Poland. An Aluminum alloy was used as raw material for 3D-printing of specimens **ALU** and **ALU-H** by means of direct metal laser sintering at Fraunhofer Ernst Mach Institute in Freiburg, Germany.

An extension test was performed on specimen **PLA**, a shearing test on specimen **PA**, and torsion tests with specimens **ALU** and **ALU-H**. In parallel, an image correlation procedure was performed. We were able to observe and to measure out-of-plane movements for specimens **PA**, **ALU**, and **ALU-H** qualitatively as well as quantitatively.

Specimen **PLA** deformed in a linear elastic way, until a first local plastic rupture occurred without resulting in total failure. This resilient deformation behavior may be used in failure-safe systems in the future to secure stability of mechanical systems, *e.g.*, in aircraft or automobile applications. In contrast to investigations that can be found in [34], out-of-plane buckling was observed during shearing tests applied to specimen **PLA**, due to the non-perfect pivots/joints. Independently, the aforementioned resilient deformation behavior was also observed for this shearing test. The untreated specimen, **ALU**, was able to carry 16% higher rotational loads during torsion tests then the heat-treated

one, **ALU-H**. Nevertheless, specimen **ALU** failed after about one total rotation in contrast to specimen **ALU-H**, which was able to resist total failure during the whole experiment ending after 5.7 total rotations. Furthermore, a reverse POYNTING effect and extraordinary nonlinear deformation behavior was observed and is further discussed in [28] and [12].

One may say that because this structure stays in the elastic range, even at large deformations, it will play a crucial role in the future in different kind of industrial applications. Its light weight in combination with its high resilient deformation behavior makes this kind of meta-material very attractive to applications in industry (*e.g.*, for protection shields in civil or defense industries, damping or mounting device for aircraft or automobile industries).

Acknowledgement. We want to thank Dag Wulsten from the Julius Wolf Institute at Charité in Berlin, Germany, and Paul Zaslansky from the Zahnklinik at Charité in Berlin, Germany, for their support and help in the lab.

References

1. Abali, B.E., Müller, W.H., Eremeyev, V.A.: Strain gradient elasticity with geometric nonlinearities and its computational evaluation. *Mech. Adv. Mater. Mod. Process.* **1**, 1–11 (2015)
2. Abali, B.E., Müller, W.H., dell’Isola, F.: Theory and computation of higher gradient elasticity theories based on action principles. *Arch. Appl. Mech.* **87**, 1495–1510 (2017)
3. Barchiesi, E., Spagnuolo, M., Placidi, L.: Mechanical metamaterials: a state of the art. *Math. Mech. Solids* **24**, 212–234 (2018)
4. Barchiesi, E., Ganzosch, G., Liebold, C., Placidi, L., Grygoruk, R., Müller, W.H.: Out-of-plane buckling of pantographic fabrics in displacement-controlled shear tests: experimental results and model validation. *Continuum Mech. Thermodyn.* (2018)
5. Chen, C., Fleck, N.A.: Size effects in the constrained deformation of metallic foams. *J. Mech. Phys. Solids* **50**, 955–977 (2002)
6. Cosserat, E., Cosserat, F.: Sur la theorie de l’elasticite. *Mathematiques, Premier memoire. Annales de la Faculte des sciences de Toulouse* (1896)
7. Cosserat, E., Cosserat, F.: *Théorie des corps déformables* (1909)
8. dell’Isola, F., Lekszycki, T., Pawlikowski, M., Grygoruk, R., Greco, L.: Designing a light fabric metamaterial being highly macroscopically tough under directional extension: first experimental evidence. *Zeitschrift für angewandte Mathematik und Physik* **66**, 3473–3498 (2015)
9. dell’Isola, F., Sciarra, G., Vidoli, S.: Generalized Hooke’s law for isotropic second gradient materials. In: *Proceedings of the Royal Society of London A: Mathematical, Physical and Engineering Sciences* (2009)
10. dell’Isola, F., Cuomo, M., Greco, L., Della Corte, A.: Bias extension test for pantographic sheets: numerical simulations based on second gradient shear energies. *J. Eng. Math.* **103**, 127–157 (2017)
11. dell’Isola, F., Turco, E., Misra, A., Vangelatos, Z., Grigoropoulos, C., Melissinaki, V., Farsari, M.: Force-displacement relationship in micro-metric pantographs: experiments and numerical simulations. *C. R. Mec.* **347**, 397–405 (2019)

12. Bachurikhin, V.P., Keller, I., Merzlyakov, A.F., Yurlov, M.A.: Experimental study of nonlinear effects under torsion of the uniform cylinder with initially circular cross section. In: *Solid State Phenomena* (2015)
13. Eringen, A.C., Suhubi, E.S.: Nonlinear theory of simple micro-elastic solids–I. *Int. J. Eng. Sci.* **2**, 189–203 (1964)
14. Eringen, A.C.: *Mechanics of micromorphic continua*. In: *Mechanics of Generalized Continua*. Springer (1968)
15. Ganzosch, G., dell’Isola, F., Turco, E., Lekszycki, T., Müller, W.H.: Shearing tests applied to pantographic structures. *Acta Polytech. CTU Proc.* **7**, 1–6 (2017)
16. Ganzosch, G., Hoschke, K., Lekszycki, T., Giorgio, I., Turco, E., Müller, W.H.: 3D-measurements of 3D-deformations of pantographic structures. *Tech. Mechanik* **38**, 233–245 (2018)
17. Gibson, L.J., Ashby, M.F.: *Cellular Solids: Structure and Properties*. Cambridge University Press (1999)
18. Gibson, L.J.: Biomechanics of cellular solids. *J. Biomech.* **38**, 377–399 (2005)
19. Juritzka, A., Yang, H., Ganzosch, G.: Qualitative investigations of experiments performed on 3D-FDM-printed pantographic structures made out of PLA. In: *New Achievements in Continuum Mechanics and Thermodynamics*. Springer (2019)
20. Kong, S., Zhou, S., Nie, Z., Wang, K.: Static and dynamic analysis of micro beams based on strain gradient elasticity theory. *Int. J. Eng. Sci.* **47**, 487–498 (2009)
21. Lakes, R.S.: Experimental microelasticity of two porous solids. *Int. J. Solids Struct.* **22**, 55–63 (1986)
22. Lakes, R.S., Drugan, W.J.: Bending of a cosserat elastic bar of square cross section: theory and experiment. *J. Appl. Mech* (2015)
23. Lam, D.C.C., Yang, F., Chong, A.C.M., Wang, J., Tong, P.: Experiments and theory in strain gradient elasticity. *J. Mech. Phys. Solids* **51**, 1477–1508 (2003)
24. Liebold, C., Müller, W.H.: Measuring material coefficients of higher gradient elasticity by using AFM techniques and Raman-Spectroscopy. In: *Generalized Continua as Models for Materials*. Springer (2013)
25. Liebold, C., Müller, W.H.: Applications of higher-order continua to size effects in bending: theory and recent experimental results. In: *Generalized Continua as Models for Classical and Advanced Materials*. Springer (2016)
26. Liebold, C.: *Größeneffekt in der Elastizität*. Dissertation Technische Universität. Berlin (2015)
27. Mindlin, R.D., Eshel, N.N.: On first strain-gradient theories in linear elasticity. *Int. J. Solids Struct.* **4**, 109–124 (1968)
28. Misra, A., Lekszycki, T., Giorgio, I., Ganzosch, G., Müller, W.H., dell’Isola, F.: Pantographic metamaterials show atypical Poynting effect reversal. *Mech. Res. Commun.* **89**, 6–10 (2018)
29. Müller, W.H., Vilchevskaya, E.N.: Micropolar theory with production of rotational inertia: a rational mechanics approach. In: *Advanced Structured Materials, Generalized Models and Non-classical Approaches in Complex Materials* (2018)
30. Müller, W.H., Vilchevskaya, E.N.: Micropolar theory from the viewpoint of mesoscopic and mixture theories. *Phys. Mesomech.* **20**, 263–279 (2017)
31. Placidi, L., Barchiesi, E., Misra, A.: A strain gradient variational approach to damage: a comparison with damage gradient models and numerical results. *Math. Mech. Complex Syst.* **6**, 77–100 (2018)
32. Placidi, L., Misra, A., Barchiesi, E.: Two-dimensional strain gradient damage modeling: a variational approach. *Z. Angew. Math. Phys.* **69**, 56 (2018)

33. Rahali, Y., Giorgio, I., Ganghoffer, J.F., Dell'Isola, F.: Homogenization a la Piola produces second gradient continuum models for linear pantographic lattices. *Int. J. Eng. Sci.* **97**, 148–172 (2015)
34. Spagnuolo, M., Barcz, K., Pfaff, A., dell'Isola, F., Franciosi, P.: Qualitative pivot damage analysis in aluminum printed pantographic sheets: numerics and experiments. *Mech. Res. Commun.* **83**, 47–52 (2017)
35. Tekoğlu, C., Onck, P.R.: Size effects in two-dimensional Voronoi foams: a comparison between generalized continua and discrete models. *J. Mecha. Phys. Solids* **56**, 3541–3564 (2008)
36. Toupin, R.A.: Elastic materials with couple-stresses. *Arch. Rational Mech. Anal.* **11**, 385–414 (1962)
37. Turco, E., dell'Isola, F., Rizzi, N.L., Grygoruk, R., Müller, W.H., Liebold, C.: Fiber rupture in sheared planar pantographic sheets: numerical and experimental evidence. *Mech. Res. Commun.* **76**, 86–90 (2016)
38. Wei, Y., Wang, X., Wu, X., Bai, Y.: Theoretical and experimental researches of size effect in micro-indentation test. *Sci. China Ser. A: Math.* **44**, 74 (2001)
39. Yang, H., Ganzosch, G., Giorgio, I., Abali, B.E.: Material characterization and computations of a polymeric metamaterial with a pantographic substructure. *Z. Angew. Math. Phys.* **69**, 105 (2018)